Sensitivity analysis of geometric error for a novel slide grinder based on improved Sobol method and its application

Dong Wang (d-wang@mail.tsinghua.edu.cn)
Tsinghua University https://orcid.org/0000-0002-4941-6862
Jihui Han
Tsinghua University
Liping Wang
Tsinghua University
Fengju Ma
Tsinghua University
Ziyang Ge
University of Electronic Science and Technology of China
Xuekun Li
Tsinghua University

Research Article

Keywords: Slide grinding, Geometric error, Sensitivity analysis, Improved Sobol method, Accuracy self-test

Posted Date: April 26th, 2022

DOI: https://doi.org/10.21203/rs.3.rs-1558167/v1

Sensitivity analysis of geometric error for a novel slide grinder based on improved Sobol method and its application

Jihui Han[1,2], Liping Wang[1,2,3], Fengju Ma[1,2,4*], Ziyang Ge[3], Dong Wang[1,2*] and Xuekun Li[1,2]

[1]State Key Laboratory of Tribology, and Institute of Manufacturing Engineering, Department of Mechanical Engineering, Tsinghua University, Beijing, 100084, China.
[2] Beijing Key Lab of Precision/Ultra-precision Manufacturing Equipment and Control, Tsinghua University, Beijing, 100084, China.
[3]School of Mechanical and Electrical Engineering, University of Electronic Science and Technology of China, Chengdu, 611731, China.
[4]Hua-Zhun Motion Co., Ltd, Jining, Shandong, 272500, China.

*Corresponding author(s). E-mail(s): mafj19@mails.tsinghua.edu.cn; d-wang@mail.tsinghua.edu.cn;

Abstract

In order to improve both the accuracy and efficiency of grinding slide, this paper designs a novel grinder with dual-lead-dual-head. Since the geometric error is one of the major contributors causing machine inaccuracies, the sensitivity analysis is performed to identify the critical geometric error terms, and an application to accuracy self-test is also given. The volumetric model of the grinder with 38 geometric errors is built by using the homogeneous transformation matrix (HTM) and multi-body system (MBS) theory. An improved Sobol method with quasi-Monte-Carlo algorithm is utilized to perform the global sensitivity analysis (GSA) in the entire workspace. The particular sensitivity analysis is further carried out on the basis of the machining characteristics of a typical slide. All sensitivity analysis results are validated through the error compensation simulations. Besides that, some discussions are given to determine the total critical errors of the grinder considering both entire workspace and particular machining requirements. Finally, the pitch and yaw errors between the dual-grinding-head are investigated, and based on the sensitivity analysis results, a quick accuracy self-test approach is proposed to reduce the measurement load in practice.

Keywords: Slide grinding, Geometric error, Sensitivity analysis, Improved Sobol method, Accuracy self-test

I Introduction

Slide is the critical part of a linear rolling guide, and the accuracy of the slide directly determines the motion smoothness and carrying ability of the linear motion axis, which further affects the performance of many types of equipment, such as CNC machine tools and coordinate measuring machines (CMMs) [1, 2]. Therefore, machining slide with high quality has always been an important goal in the industry.

Grinding is necessary for slide to achieve high accuracy, therefore, a grinder with satisfactory

performance is an essential basis. Most conventional slide grinders only have one set of motion axes and one grinding head, which needs repeated clamping to complete the grinding of different surfaces of slide, and further leads to clamping errors and reduces efficiency [3, 4]. On the other hand, the translational motion axes of these grinders are general ball screw drive systems, which only have one pitch and cannot improve the mechanical resolution and motion speed simultaneously, resulting in the contradiction between precision and efficiency [5–7]. With the rapidly growing demand for grinding accuracy and efficiency, it is significant to design a novel slide grinder to solve the above problems.

After the configuration design of a machine tool, an important task is to identify the critical geometric error terms among a large number of terms, which is the basis to guide the following manufacturing and assembly, and sensitivity analysis is necessary in this process [8]. Local sensitivity analysis (LSA) is widely used to quantify the sensitivity, and it is also known as the one-at-a-time (OAT) approach. LSA determines the sensitivity of the model output to the input parameter by calculating the partial derivative, but it examines only one parameter and takes the central value of the other parameters to evaluate the amount of variation in the output results. Although LSA is fast and easy to implement with a small amount of data, it is not applicable to nonlinear models [9]. Moreover, LSA requires prior measurement of all geometric errors of the machine tool or at least the assumptions to determine the error value, thus resulting in a deficient sensitivity analysis [10–13]. Compared with LSA, the global sensitivity analysis (GSA) is not limited to one single point but explores the whole input space, which can overcome the major limitation of LSA, such as the Morris method [14], but the method provides only semi-quantitative information without detecting and capturing interactions between parameters and nonlinearities [15, 16]. The Sobol method is another way to complete GSA, and it provides detailed information about the interactions of input parameters [17–20]. However, the normal Sobol method utilizes the pure Monte-Carlo (MC) algorithm to compute the sensitivity index of each error term [21, 22]. The base sample matrices created by the pseudo-random sequence of the method show poor uniformity, thus reducing the accuracy and efficiency of sensitivity analysis. Obviously, a better method is needed to carry out GSA to deal with complex and nonlinear geometric relations. In addition, most works of sensitivity analysis are used to determine critical error terms, beyond that, more applications could be investigated considering the characteristics of the machine tool.

Table 1: Machining process of a slide

No.	Basic Process	Equipment/Method
1	Profile stretch-bending	Outsourcing
2	Cut-off	Sawing machine
3	Rough grinding of top surface and opposite surface	Surface grinding
4	Rough grinding of both sides	Surface grinding
5	Fine-milling both end faces, punching end holes	Machining center
6	Milling cavity	Machining center
7	Tapping	Tapping Machine
8	Hardening (carburizing)	Hardening furnace
9	Sandblasting (shot blasting)	
10	Surface treatment	
11	Fine grinding of top surface	Surface grinding
12	Fine grinding of side surface	Surface grinding
13	Fine grinding of grooves	Surface grinding

In this paper, a novel grinder with dual-lead-dual-head is firstly designed to ensure the grinding accuracy and efficiency of slide. Furthermore, an improved Sobol method is presented to perform the GSA for the grinder. Considering both the entire workspace and particular machining situations of slide, the total critical error terms are investigated. Finally, based on the sensitivity analysis results, an application to accuracy self-test is proposed to reduce the measurement load for this grinder with dual-head.

The rest parts of the paper are organized as follows: Section II presents the novel dual-lead-dual-head structure; Section III describes the volumetric error model of the grinder; Section IV investigates the critical geometric error terms by applying the improved Sobol method and presents the simulation verification results; Section V gives the application to accuracy test; Section VI states the conclusion.

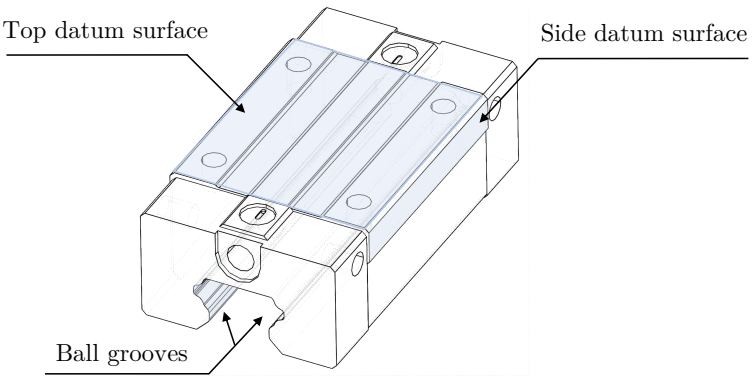

Fig. 1: The structure of a slide

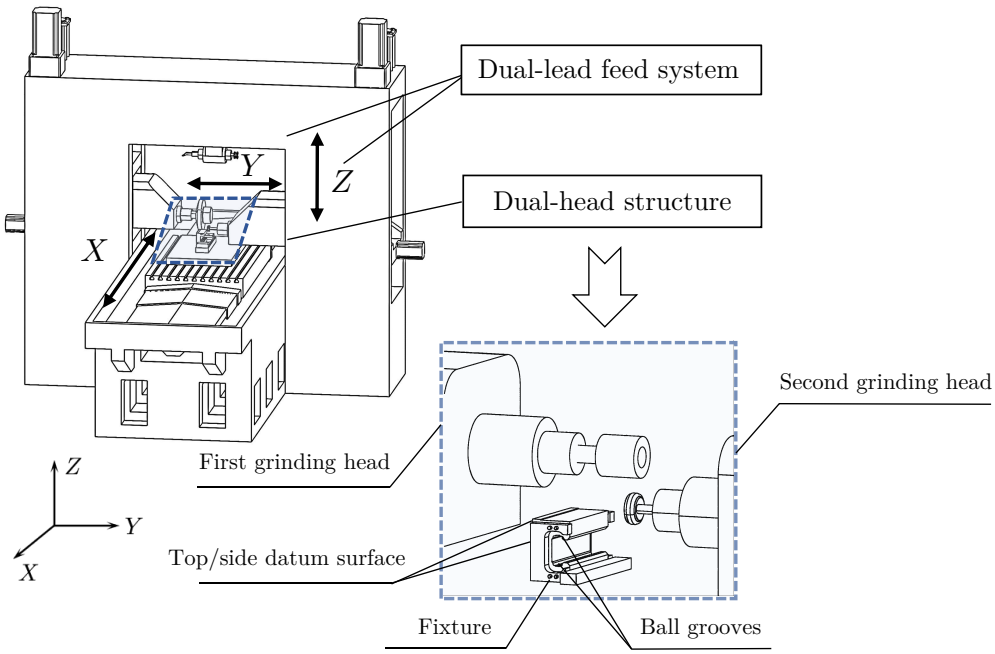

Fig. 2: The structure of dual-lead-dual-head slide grinder

II Design of the novel slide grinder

The structure diagram of a typical slide is shown in Fig. 1, and the corresponding whole machining process is listed in Table 1. The top/side datum surfaces and the ball grooves are the most important parts requiring high accuracy (i.e., 1-3 μm), thus, these three parts need fine grinding, which is also the final procedure for machining slide.

As mentioned in the Introduction, most conventional slide grinders only have one set of motion axes (i.e., X-axis, Y-axis, and Z-axis) and one grinding head. When using this kind of grinder in fine grinding procedure, repeated clamping of slide is necessary between grinding each datum surface and ball grooves. Obviously, the clamping error is unavoidable and would heavily reduce the grinding accuracy. In order to solve this problem, a novel slide grinder is designed, and the grinder has two symmetrical motion systems and two grinding heads, as shown in Fig. 2. One grinding head can be used to grind the top/side datum surfaces, and another head can be used to grind the ball grooves, therefore, the slide only needs once clamping before grinding, which completely eliminates the error caused by repeated clamping.

All translational axes of the grinder would utilize ball screw drive systems, however, conventional ball screw drive systems only have one fixed pitch, and the contradiction between motion speed and mechanical resolution always exists. For example, a large pitch could improve the motion speed, but the mechanical resolution would be reduced. On the basis of the grinder structure, a new feed system is further designed to simultaneously ensure high motion speed and high mechanical resolution, and the structure diagram is shown in Fig. 3. The feed system mainly consists of a main screw, two nuts, two worktables, and several slides. The main screw has a large pitch to achieve high motion speed, and the first nut is specially machined with thread on its outer surface. The second nut is a rotation nut to match the first nut, and the pitch of the thread is small. During the motion process, the fast feed can be ensured through the main screw with a large pitch, and the accurate feed with high mechanical resolution can be realized through the nuts with a small pitch, therefore, the contradiction between motion speed and mechanical resolution can be solved. In addition, compared with other macro-micro feed systems [23–25], the two worktables of the proposed feed system share the same guide rails, which improve the stiffness of the whole system.

Although the new feed system could improve the accuracy and efficiency of the grinder in theory, it has more components than regular ball screw drive system, and further leads to more difficulties for geometric error analysis, such as more complex models and more error terms. In subsequent sections, the modeling and sensitivity analysis of geometric error would be investigated.

III Geometric error modeling

Geometric error modeling is an important basis for carrying out precision design and error compensation. Based on the geometric error model, sensitivity analysis can be further implemented to clarify the interrelationship between geometric error terms and search for critical errors in the design phase.

The designed grinder comprises a bed, X-axis, a worktable, two symmetrical motion axes, and each set of motion axes contains Y_1-axis, Y_2-axis, Z_1-axis, Z_2-axis, and a grinding head. Each axis

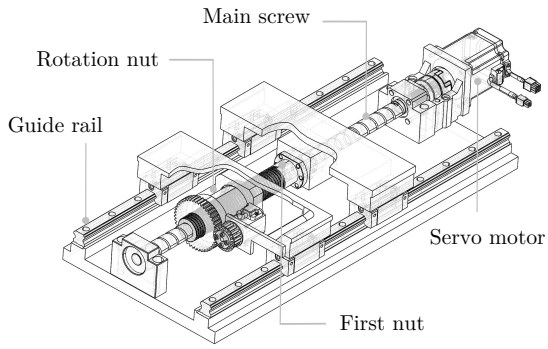

Fig. 3: The structure of dual-lead linear feed system

has six geometric error terms, including linear and angular errors. For the translational axis, the error terms comprise one positioning error, two straightness errors, and three angular errors (denoted as pitch, yaw, and roll). The rotation axis includes three linear error terms, corresponding to one axial error and two radial errors, and three angular error terms. In addition, eight squareness errors between axis pairs are considered. Considering the symmetrical structure of the grinder, only one set of motion axes needs to be analyzed, and it means a total of 38 geometric errors, which are labeled in Table 2. $\delta_i(j)$ denotes the positional error for the j-axis direction along the i-axis; $\varepsilon_i(j)$ refers to the angular error, where j-axis shows the rotation axis and i-axis shows the direction of error ($i = x, y, z$; $j = x, y_1, y_2, z_1, z_2$). The kinematic motion chain with error terms is shown in Fig. 4, where the grinding head is at the end of the kinematic chain. According to the theory of multi-body system (MBS), the kinematic coordinate relationship between two adjacent bodies can be represented by a 4×4 homogeneous transformation matrix (HTM), and the transformation matrix between two adjacent bodies can be divided into four parts: a position transformation matrix $\boldsymbol{T}_{ij}^{p}$, where notation i is the lower-order body of j; a position error transformation matrix $\Delta\boldsymbol{T}_{ij}^{p}$ (listed in Table 3); a motion transformation matrix $\boldsymbol{T}_{ij}^{s}$; a motion error transformation matrix $\Delta\boldsymbol{T}_{ij}^{s}$ (listed in Table 4).

The topological structure of the grinder including a workpiece branch and a tool branch is established as shown in Fig. 5. Each rigid body is represented by a number, where the bed is set as inertial reference frame and expressed as the "0" body, "1" represents the worktable, "2" represents

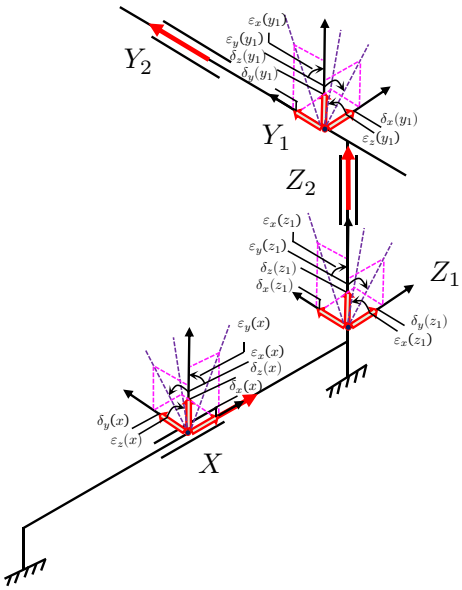

Fig. 4: Kinematic chain marked with error terms

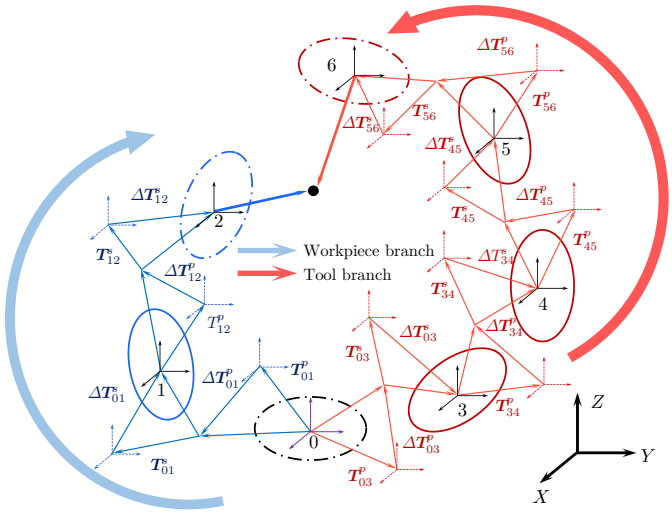

Fig. 5: Topological structure of the grinder (0-bed, 1-worktable, 2-workpiece, 3-Z_1-axis, 4-Z_2-axis, 5-Y_1-axis, 6-Y_2-axis)

Table 2: Geometric error of the slide grinder

Axis	Positioning error	Straightness error	Angular error	Squareness error
X-axis	$\delta_x(x)$	$\delta_y(x), \delta_z(x)$	$\varepsilon_x(x), \varepsilon_y(x), \varepsilon_z(x)$	
Y_1-axis	$\delta_y(y_1)$	$\delta_x(y_1), \delta_z(y_1)$	$\varepsilon_x(y_1), \varepsilon_y(y_1), \varepsilon_z(y_1)$	$S_{xy_1}, S_{xy_2}, S_{xz_1},$
Y_2-axis	$\delta_y(y_2)$	$\delta_x(y_2), \delta_z(y_2)$	$\varepsilon_x(y_2), \varepsilon_y(y_2), \varepsilon_z(y_2)$	$S_{xz_2}, S_{y_1z_1}, S_{y_1z_2},$
Z_1-axis	$\delta_z(z_1)$	$\delta_x(z_1), \delta_y(z_1)$	$\varepsilon_x(z_1), \varepsilon_y(z_1), \varepsilon_z(z_1)$	$S_{y_2z_1}, S_{y_2z_2}$
Z_2-axis	$\delta_z(z_2)$	$\delta_x(z_2), \delta_y(z_2)$	$\varepsilon_x(z_2), \varepsilon_y(z_2), \varepsilon_z(z_2)$	

the workpiece, "3" represents the Z_1-axis, "4" represents the Z_2-axis, "5" represents the Y_1-axis, "6" represents the Y_2-axis. Each rigid body has its own local coordinate system. The local coordinate systems of the end of bodies "2" and "6" are tool and workpiece coordinates, respectively.

Suppose $\boldsymbol{P}_t$ denotes the grinding point in the tool coordinate, and $\boldsymbol{P}_w$ represents the grinding point in the workpiece coordinate as

$$\boldsymbol{P}_t = [P_{tx} \;\; P_{ty} \;\; P_{tz} \;\; 1]^T \tag{1}$$

$$\boldsymbol{P}_w = [P_{wx} \;\; P_{wy} \;\; P_{wz} \;\; 1]^T \tag{2}$$

According to the topological structure of the grinder, the actual movement of the grinding head can be calculated through the product of the error transformation matrices as

$$\begin{aligned}
\boldsymbol{P}_{\text{actual}} &= [\Delta \boldsymbol{T}_{02}]^{-1} \Delta \boldsymbol{T}_{04} \Delta \boldsymbol{T}_{46} \boldsymbol{P}_t \\
\Delta \boldsymbol{T}_{02} &= \boldsymbol{T}^p_{01} \Delta \boldsymbol{T}^p_{01} \boldsymbol{T}^s_{01} \Delta \boldsymbol{T}^s_{01} \boldsymbol{T}^p_{12} \Delta \boldsymbol{T}^p_{12} \boldsymbol{T}^s_{12} \Delta \boldsymbol{T}^s_{12} \\
\Delta \boldsymbol{T}_{04} &= \boldsymbol{T}^p_{03} \Delta \boldsymbol{T}^p_{03} \boldsymbol{T}^s_{03} \Delta \boldsymbol{T}^s_{03} \boldsymbol{T}^p_{34} \Delta \boldsymbol{T}^p_{34} \boldsymbol{T}^s_{34} \boldsymbol{T}^s_{34} \\
\Delta \boldsymbol{T}_{46} &= \Delta \boldsymbol{T}^p_{45} \Delta \boldsymbol{T}^p_{45} \boldsymbol{T}^s_{45} \Delta \boldsymbol{T}^s_{45} \boldsymbol{T}^p_{56} \Delta \boldsymbol{T}^p_{56} \boldsymbol{T}^s_{56} \Delta \boldsymbol{T}^s_{56}
\end{aligned} \tag{3}$$

Similarly, the ideal movement of the grinding head can also be expressed by the product of the transformation matrix without considering the 38 geometric errors as

Table 3: Position and position error transformation matrices for the slide grinder

Axis	Position transformation matrix	Position error transformation matrix
X-axis	$\boldsymbol{T}_{01}^{p} = \boldsymbol{I}_{4\times4}$	$\Delta\boldsymbol{T}_{01}^{p} = \boldsymbol{I}_{4\times4}$
	$\boldsymbol{T}_{12}^{p} = \boldsymbol{I}_{4\times4}$	$\Delta\boldsymbol{T}_{12}^{p} = \boldsymbol{I}_{4\times4}$
Z_1-axis	$\boldsymbol{T}_{03}^{p} = \boldsymbol{I}_{4\times4}$	$\Delta\boldsymbol{T}_{03}^{p} = \begin{bmatrix} 1 & -S_{xz_1} & 0 & 0 \\ S_{xz_1} & 1 & 0 & 0 \\ 0 & 0 & 1 & 0 \\ 0 & 0 & 0 & 1 \end{bmatrix}$
Z_2-axis	$\boldsymbol{T}_{34}^{p} = \boldsymbol{I}_{4\times4}$	$\Delta\boldsymbol{T}_{34}^{p} = \begin{bmatrix} 1 & -S_{xz_2} & 0 & 0 \\ S_{xz_2} & 1 & 0 & 0 \\ 0 & 0 & 1 & 0 \\ 0 & 0 & 0 & 1 \end{bmatrix}$
Y_1-axis	$\boldsymbol{T}_{45}^{p} = \boldsymbol{I}_{4\times4}$	$\Delta\boldsymbol{T}_{45}^{p} = \begin{bmatrix} 1 & 0 & S_{xy_1} & 0 \\ 0 & 1 & -S_{y_1z_{1(2)}} & 0 \\ -S_{xy_1} & S_{y_1z_{1(2)}} & 1 & 0 \\ 0 & 0 & 0 & 1 \end{bmatrix}$
Y_2-axis	$\boldsymbol{T}_{56}^{p} = \boldsymbol{I}_{4\times4}$	$\Delta\boldsymbol{T}_{56}^{p} = \begin{bmatrix} 1 & 0 & S_{xy_2} & 0 \\ 0 & 1 & -S_{y_2z_{1(2)}} & 0 \\ -S_{xy_2} & S_{y_2z_{1(2)}} & 1 & 0 \\ 0 & 0 & 0 & 1 \end{bmatrix}$

$$\begin{aligned} \boldsymbol{P}_{\text{ideal}} &= [\boldsymbol{T}_{02}]^{-1}\boldsymbol{T}_{06}\boldsymbol{P}_t \\ \boldsymbol{T}_{02} &= \boldsymbol{T}_{01}^{p}\boldsymbol{T}_{01}^{s}\boldsymbol{T}_{12}^{p}\boldsymbol{T}_{12}^{s} \\ \boldsymbol{T}_{06} &= \boldsymbol{T}_{03}^{p}\boldsymbol{T}_{03}^{s}\boldsymbol{T}_{34}^{p}\boldsymbol{T}_{34}^{s}\boldsymbol{T}_{45}^{p}\boldsymbol{T}_{45}^{s}\boldsymbol{T}_{56}^{p}\boldsymbol{T}_{56}^{s} \end{aligned} \tag{4}$$

Based on Eq. 3 and Eq. 4, the comprehensive volumetric error can be obtained by comparing the actual and ideal positions of the grinding point, as shown in Eq. 5.

$$\boldsymbol{E} = [E_X, E_Y, E_Z, 1]^T = \boldsymbol{P}_{\text{actual}} - \boldsymbol{P}_{\text{ideal}} \tag{5}$$

where E_X, E_Y and E_Z are the components of volumetric error $\boldsymbol{E}$ in the X-, Y- and Z-directions, respectively. Volumetric error can be expressed by the function of error terms as:

$$\boldsymbol{E} = f[\delta_i(j), \varepsilon_i(j), S] \tag{6}$$

with $i = x, y, z;\ j = x, y_1, y_2, z_1, z_2$

where $\delta_i(j)$ denote the positional errors, $\varepsilon_i(j)$ denote the angular errors, S denote the squareness errors.

Finally, the scale of volumetric error E_T can be expressed as

$$E_T = \sqrt{{E_X}^2 + {E_Y}^2 + {E_Z}^2} \tag{7}$$

The volumetric error model derived in this section is the prerequisite and basis for the subsequent geometric error sensitivity analysis.

IV Sensitivity analysis of geometric error

A Sensitivity analysis approach based on improved Sobol method

In this study, based on normal Sobol method [21, 22], an improved one is utilized to complete the GSA of the slide grinder to reveal the dominant geometric error terms and also determine the interaction between each term. An overview of the improved Sobol method is provided in Fig. 6. As can be seen, the established volumetric error model can be expressed as

$$\begin{aligned} Y &= f(\boldsymbol{e}) \\ \boldsymbol{e} &= (e_1, e_2, \ldots, e_i, \ldots, e_k) \in \mathbb{R}^k \end{aligned} \tag{8}$$

where Y is defined as a scalar output, and vector $\boldsymbol{e}$ summarizes the independent model input parameters $e_1, \ldots, e_k$. In this study, $\mathbb{R}^k$ represents

Table 4: Motion and motion error transformation matrices for the slide grinder

Axis	Position transformation matrix	Position error transformation matrix
X-axis	$\boldsymbol{T}_{01}^{s} = \begin{bmatrix} 1 & 0 & 0 & x \\ 0 & 1 & 0 & 0 \\ 0 & 0 & 1 & 0 \\ 0 & 0 & 0 & 1 \end{bmatrix}$	$\Delta\boldsymbol{T}_{01}^{s} = \begin{bmatrix} 1 & -\varepsilon_z(x) & \varepsilon_y(x) & \delta_x(x) \\ \varepsilon_z(x) & 1 & -\varepsilon_x(x) & \delta_y(x) \\ -\varepsilon_y(x) & \varepsilon_x(x) & 1 & \delta_z(x) \\ 0 & 0 & 0 & 1 \end{bmatrix}$
	$\boldsymbol{T}_{02}^{s} = \boldsymbol{I}_{4\times4}$	$\Delta\boldsymbol{T}_{02}^{s} = \boldsymbol{I}_{4\times4}$
Z_1-axis	$\boldsymbol{T}_{03}^{s} = \begin{bmatrix} 1 & 0 & 0 & 0 \\ 0 & 1 & 0 & 0 \\ 0 & 0 & 1 & z_1 \\ 0 & 0 & 0 & 1 \end{bmatrix}$	$\Delta\boldsymbol{T}_{03}^{s} = \begin{bmatrix} 1 & -\varepsilon_z(z_1) & \varepsilon_y(z_1) & \delta_x(z_1) \\ \varepsilon_z(z_1) & 1 & -\varepsilon_x(z_1) & \delta_y(z_1) \\ -\varepsilon_y(z_1) & \varepsilon_x(z_1) & 1 & \delta_z(z_1) \\ 0 & 0 & 0 & 1 \end{bmatrix}$
Z_2-axis	$\boldsymbol{T}_{34}^{s} = \begin{bmatrix} 1 & 0 & 0 & 0 \\ 0 & 1 & 0 & 0 \\ 0 & 0 & 1 & z_2 \\ 0 & 0 & 0 & 1 \end{bmatrix}$	$\Delta\boldsymbol{T}_{34}^{s} = \begin{bmatrix} 1 & -\varepsilon_z(z_2) & \varepsilon_y(z_2) & \delta_x(z_2) \\ \varepsilon_z(z_2) & 1 & -\varepsilon_x(z_2) & \delta_y(z_2) \\ -\varepsilon_y(z_2) & \varepsilon_x(z_2) & 1 & \delta_z(z_2) \\ 0 & 0 & 0 & 1 \end{bmatrix}$
Y_1-axis	$\boldsymbol{T}_{45}^{s} = \begin{bmatrix} 1 & 0 & 0 & 0 \\ 0 & 1 & 0 & y_1 \\ 0 & 0 & 1 & 0 \\ 0 & 0 & 0 & 1 \end{bmatrix}$	$\Delta\boldsymbol{T}_{45}^{s} = \begin{bmatrix} 1 & -\varepsilon_z(y_1) & \varepsilon_y(y_1) & \delta_x(y_1) \\ \varepsilon_z(y_1) & 1 & -\varepsilon_x(y_1) & \delta_y(y_1) \\ -\varepsilon_y(y_1) & \varepsilon_x(y_1) & 1 & \delta_z(y_1) \\ 0 & 0 & 0 & 1 \end{bmatrix}$
Y_2-axis	$\boldsymbol{T}_{56}^{s} = \begin{bmatrix} 1 & 0 & 0 & 0 \\ 0 & 1 & 0 & y_2 \\ 0 & 0 & 1 & 0 \\ 0 & 0 & 0 & 1 \end{bmatrix}$	$\Delta\boldsymbol{T}_{56}^{s} = \begin{bmatrix} 1 & -\varepsilon_z(y_2) & \varepsilon_y(y_2) & \delta_x(y_2) \\ \varepsilon_z(y_2) & 1 & -\varepsilon_x(y_2) & \delta_y(y_2) \\ -\varepsilon_y(y_2) & \varepsilon_x(y_2) & 1 & \delta_z(y_2) \\ 0 & 0 & 0 & 1 \end{bmatrix}$

the spatial workspace domain, therefore, all 38 error terms are considered. The core concept of the Sobol method is to decompose the variance of output Y into conditional terms as

$$\begin{aligned} V_i &= \mathbb{V}_{e_i}\left[\mathbb{E}_{\boldsymbol{e}_{\sim i}}\left(Y \mid e_i\right)\right] \\ V_{ij} &= \mathbb{V}_{e_i,X_j}\left[\mathbb{E}_{\boldsymbol{e}_{\sim i,j}}\left(Y \mid e_i, e_j\right)\right] - V_i - V_j \end{aligned} \tag{9}$$

where notation $\boldsymbol{e}_{\sim i}$ denotes the vector of all input parameters except e_i.$\mathbb{E}[\cdot]$ denotes the expectation operator, $\mathbb{V}[\cdot]$ denotes the variance operator. The first-order indices for single input S_i can be obtained by dividing the model output variance $V(Y)$ in Eq. 9 as:

$$S_i = \frac{V_i}{V} = \frac{V_{e_i}\left[\mathbb{E}_{\boldsymbol{e}_{\sim i}}\left(Y \mid e_i\right)\right]}{V(Y)} \tag{10}$$

The first-order Sobol index is typically used to identify the most influential parameters. However, the output variance $V(Y)$ is the sum of variances contributed by input parameter e_i, including interactions with other parameters. It might be involved in interactions with other parameters if it is not varied alone in the model. To comprehensively analyze the coupling effect of various parameters, an additional sensitivity measure that includes high-order interaction effects needs to be addressed. The total-order Sobol index is, therefore, defined as

$$\begin{aligned} S_{T_i} &= \frac{\mathbb{E}_{\boldsymbol{e}_{\sim i}}\left[\mathbb{V}_{e_i}\left(Y \mid \boldsymbol{e}_{\sim i}\right)\right]}{V(Y)} \\ &= 1 - \frac{V_{\boldsymbol{e}_{\sim i}}\left[\mathbb{E}_{e_i}\left(Y \mid \boldsymbol{e}_{\sim i}\right)\right]}{V(Y)} \end{aligned} \tag{11}$$

When $S_{T_i} \approx 0$, it can be concluded that e_i can be fixed arbitrarily within its input range without affecting the output variance $V(Y)$. Because

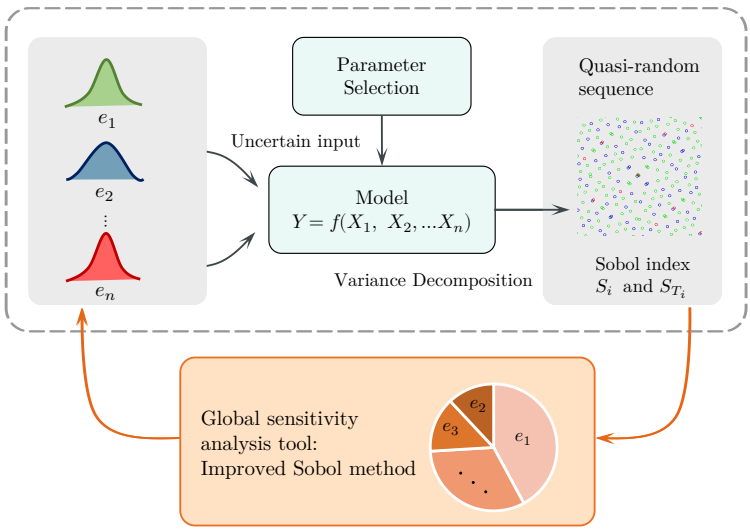

Fig. 6: Overview of sensitivity analysis based on improved Sobol method

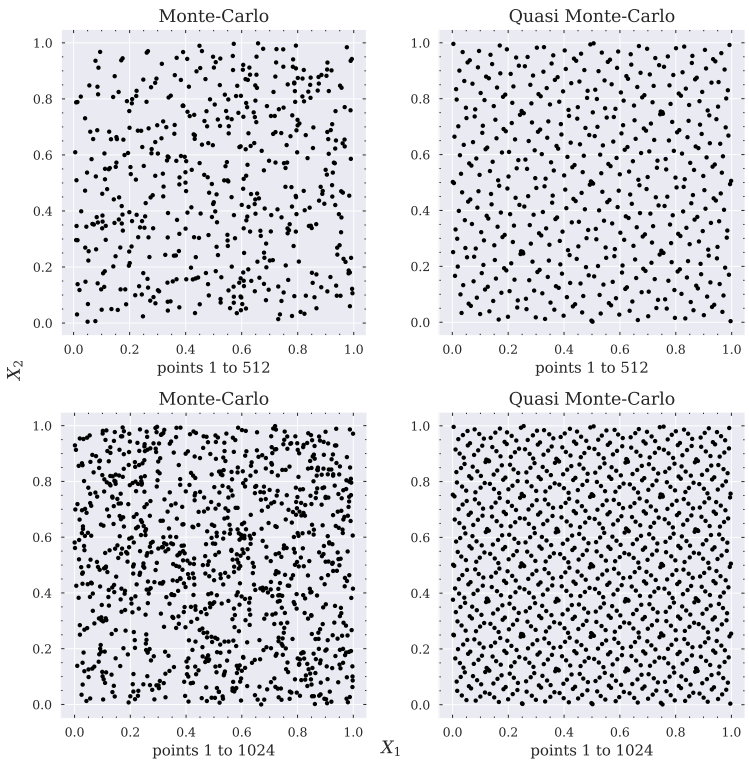

Fig. 7: Comparison between a pseudo-random point set (left) and a quasi-random point set (right) in $[0, 1]^2$, both of length $N = 2^9$

of this, total-order indices are particularly beneficial in the context of factor-fixing [15, 16]. It has been applied to distinguish between influential and non-influential model inputs, thus reducing the dimensionality of the uncertain space. Here, all sensitivity indices add up to 1 and they are all non-negative. If all 38 parameters have the same influence, each parameter can only contribute 1/38 of the variance. If few parameters are dominant to the output Y, the contribution of the remaining parameters is even smaller. The most straightforward way to compute the Sobol index is through the Monte Carlo estimation. Fourier Amplitude Sensitivity Test (FAST) can also be employed to calculate Sobol index [26]. It consists

of converting the input variable into a periodic function of a single frequency variable, and then proceeding to sample the model and analyze the sensitivity of input variables with Fourier analysis in the frequency domain. However, FAST is sensitive to the characteristic frequencies attributed to the input variable and is not straightforward as the Monte Carlo estimation does [27].

In this study, the improved Sobol method based on quasi-random sequence is used to create the training sample matrices, which is different from the normal pure Monte Carlo method based on pseudo-random sequence. Quasi-random sequence for training samples provides a better convergence in the input space, leading to a better predictive quality. Here, the two-dimensional quasi-random sequence and pseudo-random sequence on the interval $[0,1]^2$ are taken as examples to compare their distribution uniformity as shown in Fig. 7. The final number of sampling points is $N = 2^9$. It can be clearly seen that quasi-random sequences have greatly improved over pseudo-random sequences with the development of statistics. Furthermore, the comparison of statistical properties between quasi-random sequence and pseudo-random sequence is illustrated in Table 5. As can be seen, quasi-random sequence presents a better performance than pseudo-random sequence for all probabilistic distributions, indicating the improved Sobol method using the quasi-random sequence possesses higher accuracy and faster convergence speed than the normal Sobol method using the pseudo-random sequence. Therefore, the improved Sobol method would be used to identify highly sensitive geometric error terms. Finally, the estimators for S_i and S_{T_i} in Eqs. 10 and 11 can be written as:

$$\mathbb{V}_{e_i}\left[\mathbb{E}_{\boldsymbol{e}_{\sim i}}\left[Y|e_i\right]\right]=\frac{1}{N}\sum_{m=1}^{N} f(\boldsymbol{B})_m\left(f\left(\boldsymbol{A}_B^{(i)}\right)_m-f(\boldsymbol{A})_m\right) \tag{12}$$

$$\mathbb{E}_{\boldsymbol{e}_{\sim i}}\left[\mathbb{V}_{e_i}\left[Y|\boldsymbol{e}_{\sim i}\right]\right]=\frac{1}{2N}\sum_{m=1}^{N}\left(f(\boldsymbol{A})_m-f\left(\boldsymbol{A}_B^{(i)}\right)_m\right)^2 \tag{13}$$

$$V=\frac{1}{k}\sum_{m=1}^{k} f(\boldsymbol{A})_m^2-\left[\frac{1}{k}\sum_{m=1}^{k} f(\boldsymbol{A})_m\right]^2 \tag{14}$$

where a $(N, 2k)$ base sample matrix is generated by the quasi-Monte-Carlo sequence. Each row is a sampling point and each column is a model input. The first k columns are allocated to an $\boldsymbol{A}$ matrix and the remaining k columns to a $\boldsymbol{B}$ matrix. Any point in either $\boldsymbol{A}$ or $\boldsymbol{B}$ can be indicated as e_{vi}, where v and i respectively express the row (from 1 to N) and the column (from 1 to k). Then, k additional $\boldsymbol{A}_B^{(i)}\boldsymbol{B}_A^{(i)}$ matrices are created, where all columns come from $\boldsymbol{A}(\boldsymbol{B})$ except the i-th column, which comes from $\boldsymbol{B}(\boldsymbol{A})$.$S_i$ and S_{T_i} can be finally estimated using the model evaluations obtained from the combinations of the matrices $\boldsymbol{A}(\boldsymbol{B}), \boldsymbol{B}(\boldsymbol{A}), \boldsymbol{A}_B^{(i)}$ and $\boldsymbol{B}_A^{(i)}$.

Table 5: Comparison of statistical properties between quasi-random sequence and pseudo-random sequence ($N = 2^9$)

	Theoretical distribution	Quasi-random sequence	Pseudo-random sequence
Mean	0.5	0.499	0.492
Standard Deviation	0.289	0.288	0.284
Variance	0.083	0.083	0.081

B Global sensitivity analysis results

The ISO230-6 specifies body diagonal displacement tests of motion space, which allow evaluation of the volumetric performance of a machine tool [28]. A total of 17 points were selected for this study. The stroke of translational axes are $x \in [0, 650]$ mm, $y \in [0, 350]$ mm, $z \in [0, 500]$ mm. As shown in Fig. 8, five test points were uniformly selected along each body diagonal of the grinder's workspace. Point 17 is the intersection point of the body diagonals. A sensitivity analysis of the entire workspace can be obtained by adopting the average value.

In this study, the error sample ranges of positioning errors along Y_2- and Z_2-axis are set to $[-0.1, 0.1]$ µm, the positioning errors along X-, Y_1- and Z_1-axis are set to $[-1, 1]$ µm; all the linear errors except the positioning errors are set to $[-0.5, 0.5]$ µm, and all angular errors and squareness errors are set to $[-1, 1]$ µrad. The number of sampling points for each error is set to 20000. Thus, $\boldsymbol{A}$ and $\boldsymbol{B}$ described in Section IV-A are constructed as 20000×38 sampling metrics.

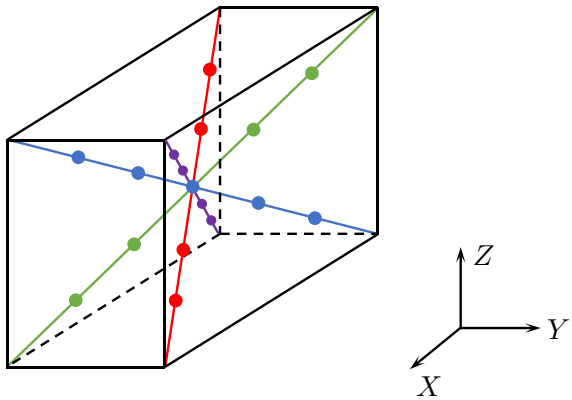

Fig. 8: 17 positions selected in the workspace of the grinder

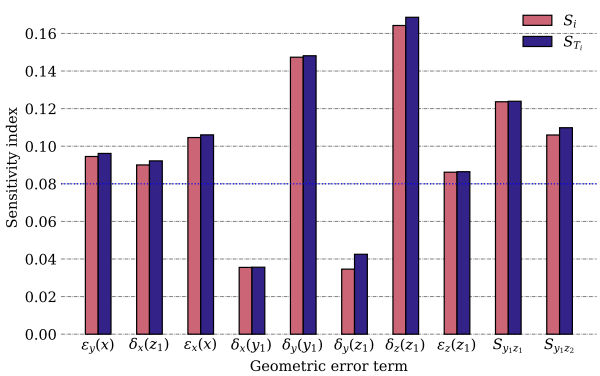

Fig. 9: Bar plots showing the sensitivity indices of volumetric error over the entire workspace

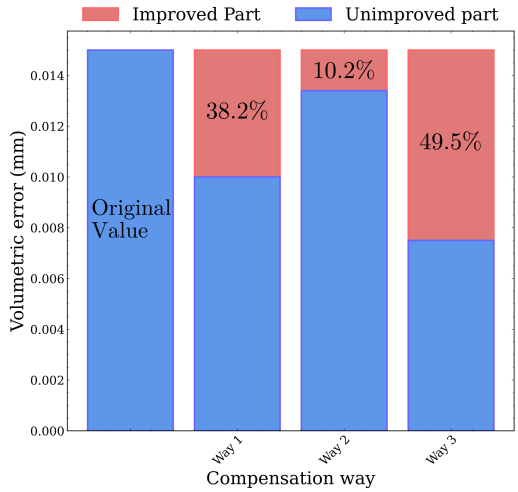

Fig. 10: Simulation result of the volumetric error over the entire workspace by different compensation ways

The calculated results of the sensitivity analysis concerning volumetric error over the entire workspace are visualized in Fig. 9. From a total of 38 geometric error terms, the 10 geometric error terms with the largest sensitivity indices were selected to create the histogram, as the rest error terms have little effect on the machining accuracy. As can be seen from Fig. 9, sensitivity indices of first-order and total-order are close to each other, which shows a slight interaction between any two arbitrary error terms. Therefore, the first-order sensitivity indices will be mainly used to distinguish the critical error terms. Among all geometric error terms of the grinder, those with first-order sensitivity indices greater than 0.08 are considered as critical sensitive error terms.

For the comprehensive volumetric model over the entire workspace, $\delta_y(y_1)$ and $\delta_z(z_1)$ have the largest first-order sensitivity values, and other critical geometric error terms are $\varepsilon_y(x), \delta_x(z_1), \varepsilon_x(x), \varepsilon_z(z_1), S_{y_1z_1}, S_{y_1z_2}$.

To verify the results of the sensitivity analysis, the geometric errors are compensated in three different ways to investigate their influences. In the validation analysis, the middle number in the positive error range was taken as a fixed value of the error. The first way is to reduce the values of critical geometric error terms to half of the original values and maintain the original values of the other geometric error terms; the second way is to maintain the values of the critical geometric error terms and reduce half the other geometric error terms from their original values; the final way is to reduce half all the geometric errors from their original values.

As shown in Fig. 10, the bar plot illustrates the average volumetric errors with different compensation ways. Based on the results, the volumetric errors are improved by 38.2%, 10.2% and 49.5% by compensating the critical error terms, other geometric error terms and all error terms. Obviously, the volumetric errors in the entire workspace can be greatly improved by only compensating the critical error terms, which indicate the effectiveness of the error sensitivity analysis in the entire workspace.

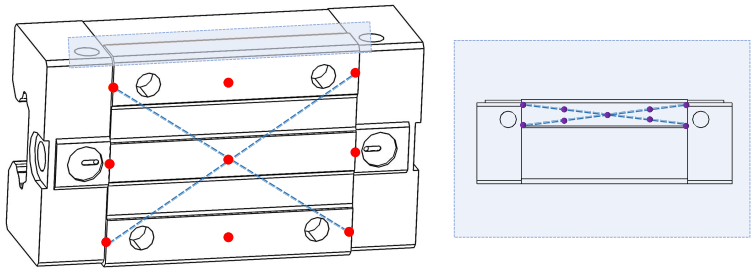

Fig. 11: Test positions selected on the top (left) and side (right) datum surfaces of a HIWIN HGH20CA slide

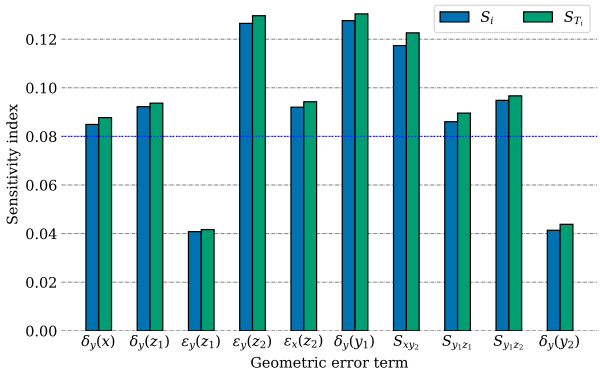

Fig. 12: Bar plots showing the geometric error sensitivity indices of typical slide surface in the Y-direction

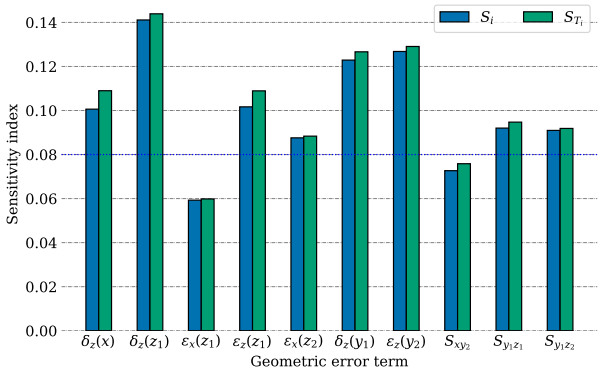

Fig. 13: Bar plots showing the geometric error sensitivity indices of typical slide surface in the Z-direction

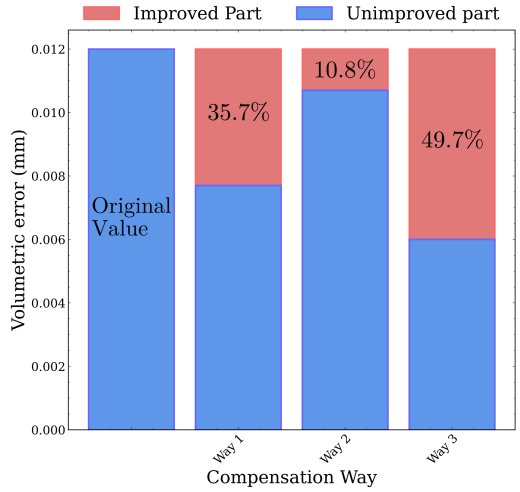

Fig. 14: Simulation result of the volumetric error along Y-direction by different compensation methods considering the machining characteristics of a typical slide

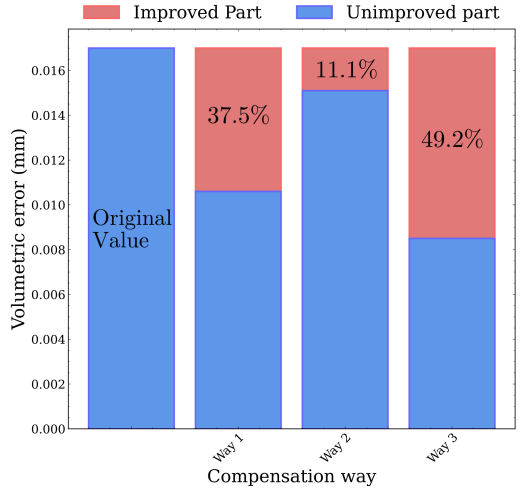

Fig. 15: Simulation result of the volumetric error along Z-direction by different compensation methods considering the machining characteristics of a typical slide

C Particular sensitivity analysis results considering machining characteristics

Besides the error sensitivity analysis in the entire workspace, a particular sensitivity analysis is further investigated considering the machining characteristics of a typical slide. In this subsection, the HIWIN HGH20CA [29] was targeted as the object of the sensitivity analysis, and the parameters of the slide are outlined in [29]. The test positions of the surface are uniformly selected as shown in Fig. 11. Red points and purple points illustrate the test points of the side datum surface and the top datum surface, respectively. Considering the structure of the slide and its corresponding machining characteristics, the volumetric error terms along the Y- and Z-directions, respectively, have a significant impact on the machining accuracy when machining the top datum surface and the side datum surface. It is therefore important to analyze the sensitivity indices for these two directions.

The same analysis method and evaluation criteria as for the comprehensive volumetric error are used to analyze the sensitivity of the error terms in the Y- and Z-directions. The sensitivity analysis result for the Y-direction is illustrated in Fig. 12. The sensitivity values of $\delta_y(y_1), \varepsilon_y(z_2)$ and S_{xy_2} are the largest, and other critical errors terms are $\delta_y(x), \delta_y(z_1), \varepsilon_x(z_2), S_{y_1z_1}, S_{y_1z_2}$. The sensitivity analysis result for the Z-direction is illustrated in Fig. 13. The sensitivity values of $\delta_z(z_1), \delta_z(y_1)$ and $\varepsilon_z(y_2)$ are the largest, and other critical error terms are $\delta_z(x), \varepsilon_z(z_1), \varepsilon_x(z_2), S_{y_1z_1}, S_{y_1z_2}$.

The validation is conducted to confirm the sensitivity analysis results, as illustrated in Figs. 14 and 15. Based on the results, the volumetric errors along Y-direction are improved by $35.7\%, 10.8\%$ and 49.7% by compensating the critical error terms, other geometric error terms and all error terms. The volumetric errors along Z-direction are improved by $37.5\%, 11.1\%$ and 49.2%. Obviously, the volumetric errors considering the machining characteristics can be greatly improved by only compensating the critical error terms, which indicate the effectiveness of the particular error sensitivity analysis considering the machining characteristics of a typical slide.

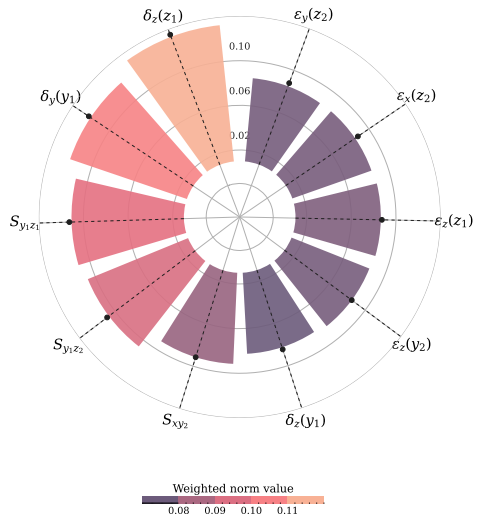

Fig. 16: Circular bar plot showing the total critical errors of the grinder considering both entire workspace and particular machining requirements

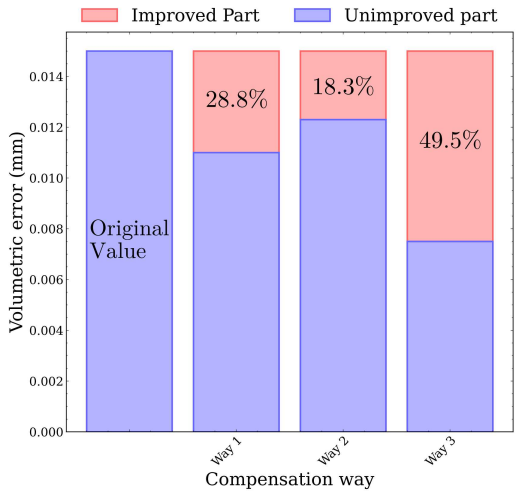

Fig. 17: Simulation result of the volumetric error by different compensation ways of the total critical error terms for the entire workspace

D Investigation of the total critical error terms

Considering above global and particular sensitivity analysis results, the total critical error terms for this novel grinder are statistically captured by calculating the weighted Euclidean norm as:

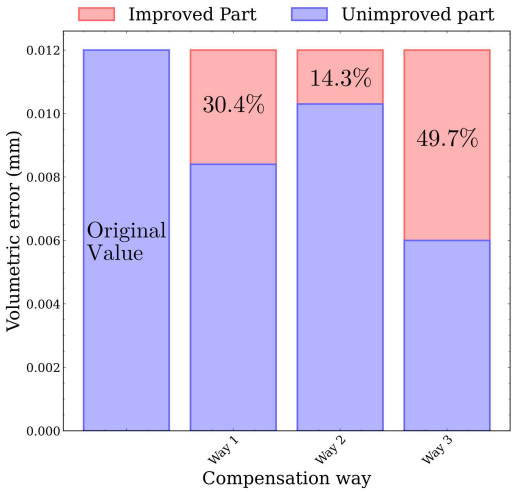

Fig. 18: Simulation result of the volumetric error along the Y-direction by different compensation ways of the total critical error terms considering the machining characteristics of typical slide

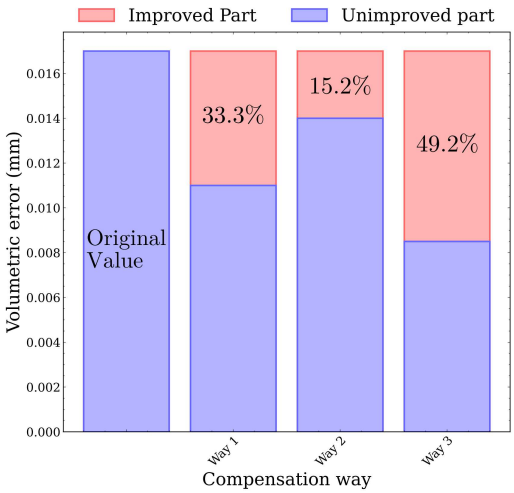

Fig. 19: Simulation result of the volumetric error along the Z-direction by different compensation ways of the total critical error terms considering the machining characteristics of typical slide

$$\|t\| = \sqrt{\sum_{i=1}^{n} w_i \left(t_i\right)^2} \qquad (15)$$
$$t = (t_1, t_2, \cdots, t_n)$$

where $\sum_{i=1}^{n} w_i = 1, \forall w_i \in [0,1], \|\cdot\|$ denotes the weighted Euclidean norm with weight w_i.

Since this grinder is designed for machining slide, the weights for particular sensitivity analysis results (i.e., Y- and Z- direction) are set slightly higher than the sensitivity analysis result over entire workspace, as

$$w = \left(\frac{3}{10}, \frac{7}{20}, \frac{7}{20}\right) \qquad (16)$$

The analysis result of 10 largest weighted norm values is visualized in Fig. 16 by using a circular bar plot. Based on the result, it can be confirmed that the sensitivity values of $\delta_z\left(z_1\right), \delta_y\left(y_1\right), S_{y_1z_1}, S_{y_1z_2}$ are the largest, therefore, these four error terms should be given priority to ensure the initial accuracy of the grinder. Other total critical error terms are $S_{xy_2}, \delta_z\left(y_1\right), \varepsilon_z\left(y_2\right), \varepsilon_z\left(z_1\right), \varepsilon_x\left(z_2\right), \varepsilon_y\left(z_2\right)$. A compensation validation is further performed to confirm that the obtained total critical error terms can characterize both the entire workspace and particular machining situations. Fig. 17 shows the volumetric error by different compensation ways of the total critical error terms for the entire workspace. Figs. 18 and 19 illustrate the volumetric error along the Y- and Z-direction by different compensation ways of the total critical error terms considering the machining characteristics of typical slide. In all three cases, although the accuracy improvement of compensating total critical error terms is not as good as compensating the critical errors obtained from respective sensitivity analysis, the values are all greater than compensating the other remaining error terms. These results demonstrate that the obtained total critical error terms can describe both the entire workspace and particular machining situations.

V Application to accuracy self-test

Based on the above sensitivity analysis results, accuracy design can be carried out to ensure that the grinder has high accuracy in the initial stage. Although the accuracy of the grinder could meet requirements in initial stage, it is unable to guarantee that the accuracy still maintains at the acceptable tolerance range after a long-term operation. In order to ensure consistent accuracy for mass slide production, it is necessary to perform periodic accuracy test and maintenance. Traditionally, all critical error terms should be tested

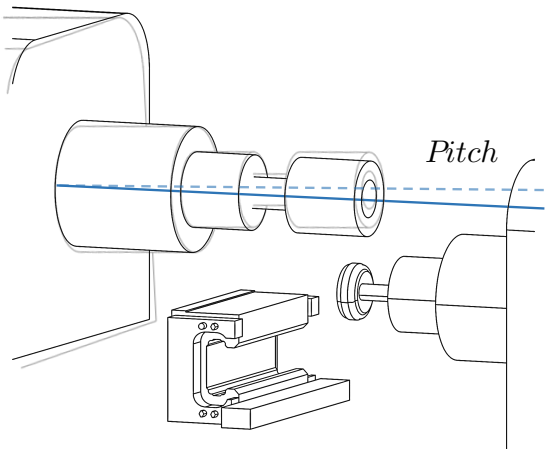

Fig. 20: The pitch error of the grinding head

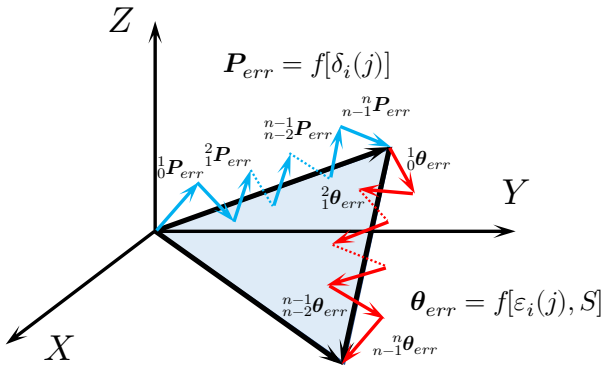

Fig. 21: Posture error caused by angular errors and squareness errors

one by one, but there are 76 error terms in total with 20 critical error terms for the novel grinder with symmetrical structure, which means a heavy measuring load in practice. In addition, among all error terms, posture errors are much more difficult to be measured than positional errors. In order to solve the above problem, a fast accuracy self-test approach is proposed based on the structural characteristics of the grinder and the error sensitivity analysis results in this section.

A Posture error of the dual-head

For the normal geometric sensitivity analysis, the error of translational axis consists of three positional errors and three angular errors, and they are not discussed separately. Since the novel grinder does not have a rotation axis, the posture error of grinding head, such as the pitch error shown in Fig. 20, is only affected by the angular geometric error of the motion axis. Hence, if the posture of the grinding head deviates angularly from its initial resting plane, it is caused by angular or squareness error. As a result, volumetric error can be divided into two parts as illustrated in Fig. 21: positional error vector $\boldsymbol{P}_{err}$ and posture error vector $\boldsymbol{\theta}_{err}$, as

$$\begin{aligned} \boldsymbol{P}_{err} &= f\left[\delta_i(j)\right] \\ \boldsymbol{\theta}_{err} &= f\left[\varepsilon_i(j), S\right] \\ \text{with } i = x, y, z;\ j &= x, y_1, y_2, z_1, z_2 \end{aligned} \tag{17}$$

where $\delta_i(j)$ denote the positional errors, $\varepsilon_i(j)$ denote the angular errors, S denote the squareness errors. According to the analysis results in Section IV-D, only three total critical error terms are angle-independent, which means that the posture error would be heavily affected by the total critical error terms. In turn, the posture error could be used to evaluate the variations of critical error terms in a large extent, which provides a possible way to achieve fast accuracy test.

B The accuracy self-test approach

A sensitivity analysis is firstly performed for the posture error of the grinding head. It is assumed that one side of the grinding head does not have any posture errors from its initial static phase. The posture error between dual grinding heads around X-direction (i.e., pitch) is examined as shown in Fig. 22. The sensitivity indices are largest with the error terms of $S_{y_1z_1}S_{y_1z_2}, \varepsilon_{\mathrm{x}}(z_2)$, and other critical errors terms are $\varepsilon_{\mathrm{y}}(z_2), \varepsilon_{\mathrm{z}}(z_1), \varepsilon_{\mathrm{z}}(\mathrm{y}_2), S_{xy_2}$, which completely covers the seven critical posture error terms in Section IV-D. Meanwhile, the posture error between dual grinding heads around Z-direction (i.e., yaw) is examined. Fig. 23 shows that $S_{y_1z_1}S_{y_1z_2}$, have the largest sensitivity values, and other critical error terms are $\varepsilon_x(x), \varepsilon_y(x), \varepsilon_z(z_1), \varepsilon_x(y_1), S_{xy_1}$, covering three critical posture error terms in Section IV-D. Considering the overlapping ratio, the pitch error shows a stronger correlation with the total critical error terms. Therefore, it is more effective to

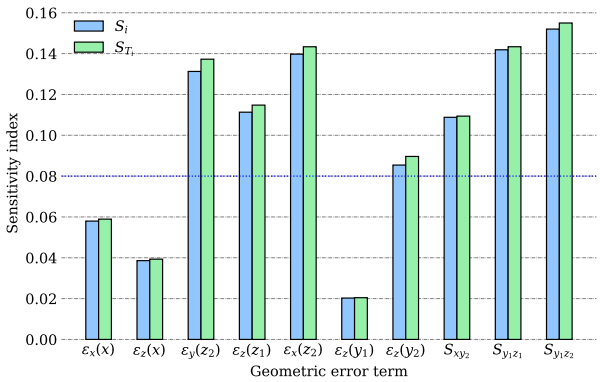

Fig. 22: Bar plots showing the sensitivity indices of posture error between dual grinding heads around X-direction

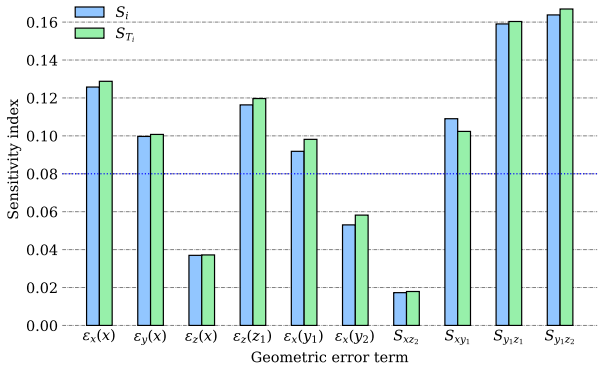

Fig. 23: Bar plots showing the sensitivity indices of posture error between dual grinding heads around Z-direction

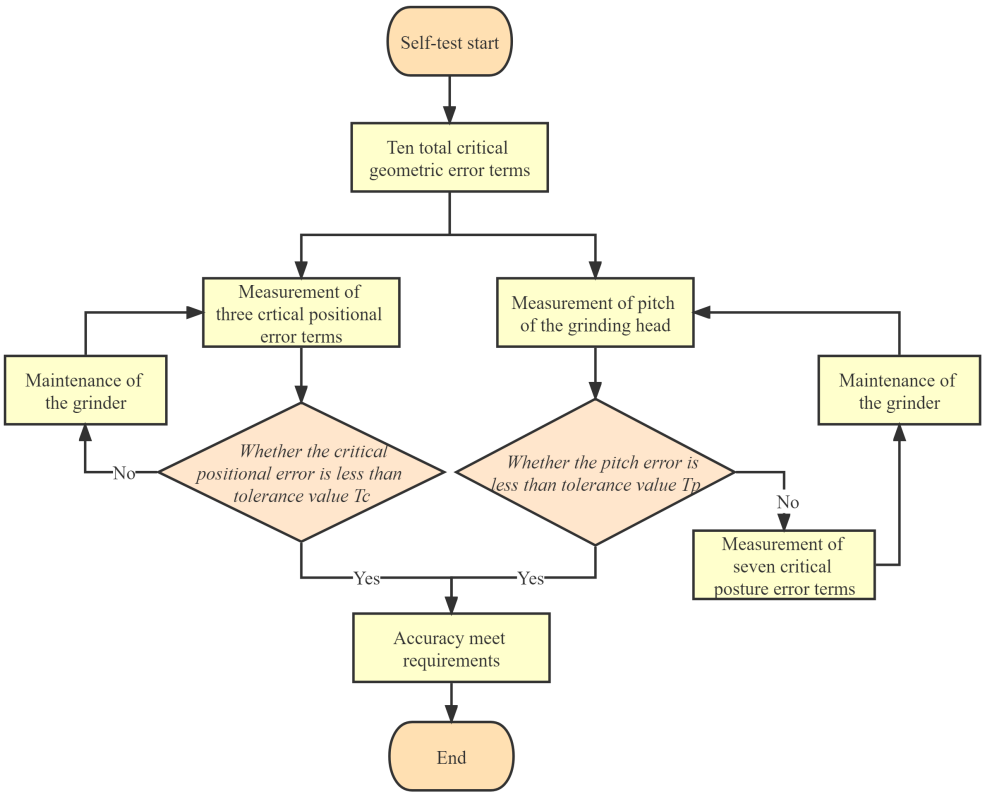

Fig. 24: Fast accuracy self-test flow

characterize the geometric accuracy by measuring the pitch error between the dual grinding heads.

Furthermore, a fast accuracy self-test approach is proposed, as shown in Fig. 24. First, the critical positional error terms (i.e., $\delta_z(z_1), \delta_y(y_1), \delta_z(y_1)$) and the pitch error between dual grinding heads are measured. If the critical positional error terms are larger than the

tolerance value T_c, then the maintenance should be performed. On the other hand, only if the pitch error of the grinding heads is larger than the tolerance value T_p, other seven critical posture error terms should be measured. In this way, the initial measurement of 10 critical error terms is reduced to 4. Also, since posture errors are much more difficult to be measured than positional errors, it saves great effort to use pitch error to represent seven critical posture errors. Based on this self-test flow, it is possible to create an automatic algorithm for engineers to check the geometric accuracy status of the grinder without measuring all the critical error terms in the beginning.

VI Conclusion

This paper designs a novel slide grinder with dual-lead-dual-head to improve both accuracy and efficiency, and the sensitivity analysis of geometric error is further investigated for the new structure. By utilizing the improved Sobol method, sensitivity analyses are conducted considering the entire workspace and typical machining characteristics, and corresponding critical error terms are obtained. Based on all analysis results for different cases, the total critical error terms are determined, and the results are validated through error compensation simulation. These analysis results could be used to help engineers with accuracy design. Moreover, an approach for accuracy self-test is proposed for the grinder, as an application of error sensitivity analysis. This approach reduces the measuring error terms from 10 to 4 in the initial stage, which improves the efficiency in practice.

Declarations

Author contribution. Methodology, validation, formal analysis, and writing—original draft preparation, J.H.; conceptualization, resources, funding acquisition, and writing—review and editing, D.W., X.L.; investigation and data curation, Z.G.; visualization, supervision, project administration, L.W. and F.M. All the authors have read and agreed to the published version of the manuscript.

Funding. This work was supported by the National Natural Science Foundation of China (Grant No. 52105520, No. 51975319), Beijing Municipal Natural Science Foundation (Grant No. 3214043) and Project of State Key Lab of Tribology of Tsinghua University (Grant No. SKLT2021D16).

Data availability. Not applicable.

Code availability. Not applicable

Conflict of interest. The authors declare no competing interests.

Ethics approval. Not applicable.

Consent to participate. Not applicable.

Consent for publication. Not applicable.

References

[1] M. Rahmani and F. Bleicher, "Experimental and numerical studies of the influence of geometric deviations in the performance of machine tools linear guides," *Procedia CIRP*, vol. 41, pp. 818–823, 2016.

[2] F. Qibo, Z. Bin, C. Cunxing, K. Cuifang, Z. Yusheng, and Y. Fenglin, "Development of a simple system for simultaneously measuring 6dof geometric motion errors of a linear guide," *Optics express*, vol. 21, no. 22, pp. 25 805–25 819, 2013.

[3] M. Zaeh, T. Oertli, and J. Milberg, "Finite element modelling of ball screw feed drive systems," *CIRP Annals*, vol. 53, no. 1, pp. 289–292, 2004.

[4] D. A. Vicente, R. L. Hecker, F. J. Villegas, and G. M. Flores, "Modeling and vibration mode analysis of a ball screw drive," *The International Journal of Advanced Manufacturing Technology*, vol. 58, no. 1, pp. 257–265, 2012.

[5] J. Kopac and P. Krajnik, "High-performance grinding—a review," *Journal of Materials Processing Technology*, vol. 175, no. 1-3, pp. 278–284, 2006.

[6] W. B. Rowe, *Principles of modern grinding technology*. William Andrew, 2013.

[7] D. Wang, S. Zhang, L. Wang, and Y. Liu, "Developing ball screw drive system of high speed machine tool considering dynamics," *IEEE Transactions on Industrial Electronics*, 2021.

[8] L. Wang, D. Wang, B. Wang, and W. Li, "Development of an oscillating grinding machine tool

based on error analysis," *Science China Technological Sciences*, vol. 63, no. 6, pp. 912–922, 2020.

[9] A. Saltelli, K. Aleksankina, W. Becker, P. Fennell, F. Ferretti, N. Holst, S. Li, and Q. Wu, "Why so many published sensitivity analyses are false: A systematic review of sensitivity analysis practices," *Environmental modelling and software*, vol. 114, pp. 29–39, 2019.

[10] J. Li, F. Xie, and X.-J. Liu, "Geometric error modeling and sensitivity analysis of a five-axis machine tool," *The International Journal of Advanced Manufacturing Technology*, vol. 82, no. 9, pp. 2037–2051, 2016.

[11] Q. Li, W. Wang, Y. Jiang, H. Li, J. Zhang, and Z. Jiang, "A sensitivity method to analyze the volumetric error of five-axis machine tool," *International Journal of Advanced Manufacturing Technology*, vol. 98, pp. 1791–1805, 9 2018.

[12] J. Fan, Q. Liu, W. Li, L. Xue, and C. Li, "Geometric error modeling and sensitivity analysis of cnc internal circular compound grinding machine," *International Journal of Mechanical Engineering and Applications*, vol. 8, p. 118, 2020.

[13] P. Niu, Q. Cheng, Z. Liu, and H. Chu, "A machining accuracy improvement approach for a horizontal machining center based on analysis of geometric error characteristics," *The International Journal of Advanced Manufacturing Technology*, vol. 112, 02 2021.

[14] M. D. Morris, "Factorial sampling plans for preliminary computational experiments," *Technometrics*, vol. 33, no. 2, pp. 161–174, 1991.

[15] A. Saltelli, S. Tarantola, F. Campolongo, and M. Ratto, *Sensitivity analysis in practice: a guide to assessing scientific models*. Wiley Online Library, 2004, vol. 1.

[16] A. Saltelli, M. Ratto, T. Andres, F. Campolongo, J. Cariboni, D. Gatelli, M. Saisana, and S. Tarantola, *Global sensitivity analysis: the primer*. John Wiley & Sons, 2008.

[17] S. Guo, D. Zhang, and Y. Xi, "Global quantitative sensitivity analysis and compensation of geometric errors of cnc machine tool," *Mathematical Problems in Engineering*, vol. 2016, 2016.

[18] X. Zou, X. Zhao, G. Li, Z. Li, and T. Sun, "Sensitivity analysis using a variance-based method for a three-axis diamond turning machine," *International Journal of Advanced Manufacturing Technology*, vol. 92, pp. 4429–4443, 10 2017.

[19] X. Zou, X. Zhao, Z. Wang, G. Li, Z. Hu, and T. Sun, "Error distribution of a 5-axis measuring machine based on sensitivity analysis of geometric errors," *Mathematical Problems in Engineering*, vol. 2020, 2020.

[20] X. Jiang, Z. Cui, L. Wang, C. Liu, M. Li, J. Liu, and Y. Du, "Critical geometric errors identification of a five-axis machine tool based on global quantitative sensitivity analysis," *International Journal of Advanced Manufacturing Technology*, 2022.

[21] I. M. Sobol', "On sensitivity estimation for nonlinear mathematical models," *Matematicheskoe modelirovanie*, vol. 2, no. 1, pp. 112–118, 1990.

[22] I. M. Sobol, "Global sensitivity indices for nonlinear mathematical models and their monte carlo estimates," *Mathematics and computers in simulation*, vol. 55, no. 1-3, pp. 271–280, 2001.

[23] L. N. Sun, D. G. Jie, Y. J. Liu, Z. C. Chen, and H. G. Cai, "Investigation on a novel dual-grating macro-micro driven high speed precision positioning system for nems," in *2006 1st IEEE International Conference on Nano/Micro Engineered and Molecular Systems*. IEEE, 2006, pp. 644–648.

[24] C. Yang, G. L. Wang, B. S. Yang, and H. R. Wang, "Research on the structure of high-speed large-scale ultra-precision positioning system," in *2008 3rd IEEE International Conference on Nano/Micro Engineered and Molecular Systems*. IEEE, 2008, pp. 9–12.

[25] L. Zhang, J. Gao, X. Chen, Y. Chen, Y. He, Y. Zhang, H. Tang, and Z. Yang, "Implementation and experiment of an active vibration reduction strategy for macro-micro positioning system," *Precision Engineering*, vol. 51, pp. 319–330, 2018.

[26] A. Saltelli and R. Bolado, "An alternative way to compute fourier amplitude sensitivity test (fast)," *Computational Statistics & Data Analysis*, vol. 26, no. 4, pp. 445–460, 1998.

[27] A. Saltelli, P. Annoni, I. Azzini, F. Campolongo, M. Ratto, and S. Tarantola, "Variance based sensitivity analysis of model output. design and estimator for the total sensitivity index," *Computer physics communications*, vol. 181, no. 2, pp. 259–270, 2010.

[28] I. 230-6, "Test code for machine tools, part 6: determination of positioning accuracy on body and face diagonals (diagonal displacement tests)," 2002.

[29] "Hgh20ca." [Online]. Available: http://www.hiwin.sc.cn/HIWIN/HG/HGH20CA.html